THE JOURNAL OF PHYSICAL CHEMISTRY B

Article

Cite This: J. Phys. Chem. B 2018, 122, 7616−7624

pubs.acs.org/JPCB

X-ray Scattering and O−O Pair-Distribution Functions of Amorphous Ices

Daniel Mariedahl,[†] Fivos Perakis,[†] Alexander Späh,[†] Harshad Pathak,[†] Kyung Hwan Kim,[†] Gaia Camisasca,[†] Daniel Schlesinger,[‡,§] Chris Benmore,[⊥] Lars Gunnar Moody Pettersson,[†] Anders Nilsson,[†] and Katrin Amann-Winkel*[,†]

[†]Department of Physics, AlbaNova University Center, Stockholm University, SE-10691 Stockholm, Sweden

[‡]Department of Environmental Science and Analytical Chemistry (ACES), and [§]Bolin Centre for Climate Research, Stockholm University, SE-11418 Stockholm, Sweden

[⊥]X-ray Science Division, Advanced Photon Source, Argonne National Laboratory, Argonne, Illinois 60439, United States

Supporting Information

ABSTRACT: The structure factor and oxygen−oxygen pair-distribution functions of amorphous ices at liquid nitrogen temperature (T = 77 K) have been derived from wide-angle X-ray scattering (WAXS) up to interatomic distances of r = 23 Å, where local structure differences between the amorphous ices can be seen for the entire range. The distances to the first coordination shell for low-, high-, and very-high-density amorphous ice (LDA, HDA, VHDA) were determined to be 2.75, 2.78, and 2.80 Å, respectively, with high accuracy due to measurements up to a large momentum transfer of 23 Å^{-1}. Similarities in pair-distribution functions between LDA and supercooled water at 254.1 K, HDA and liquid water at 365.9 K, and VHDA and high-pressure liquid water were found up to around 8 Å, but beyond that at longer distances, the similarities were lost. In addition, the structure of the high-density amorphous ices was compared to high-pressure crystalline ices IV, IX , and XII, and conclusions were drawn about the local ordering.

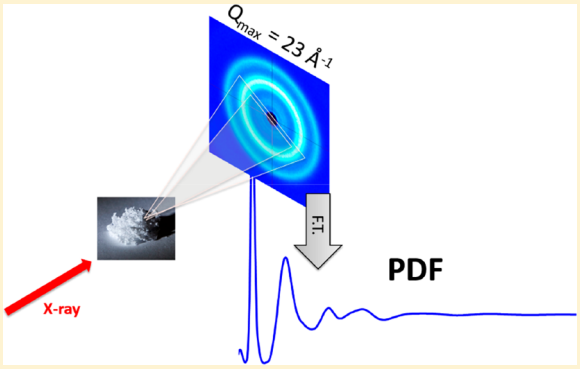

INTRODUCTION

Water is an important and unique liquid exhibiting many different anomalies upon supercooling, such as a seemingly diverging isothermal compressibility, heat capacity, and expansion coefficient.[1,2] Explaining this anomalous behavior of water is a major challenge that has given rise to controversial discussions over decades.[3−5] Experimental observations of two distinct amorphous states of ice and a first-order transition between them,[6] high- and low-density amorphous (HDA, LDA), and theoretical considerations[7−9] have led to a picture of water as "two liquids".[3,10] In this picture, the local structure of ambient liquid water fluctuates between two distinct local molecular motifs.[2] One scenario suggests that liquid water can exist in two different forms in the metastable part of the phase diagram below the temperature of homogeneous ice nucleation, namely, high- and low-density liquid water (HDL and LDL),[7,8] with the coexistence line ending at the so-called second critical point. In this part of the phase region, experimental investigations of the two potential liquid states become extremely challenging due to crystallization. Experimentally better accessible are the two amorphous states of water HDA and LDA, which are believed to be the glassy counterparts of the two liquid states, but this issue is also controversially debated.[11] It should be noted that slight variations in properties within these two classes of amorphous ice may occur due to the sample history, as discussed below. For LDA-type ices, an experimental observation of a glass transition has been reported[12] for samples prepared through vapor deposition and through hyperquenching liquid water.[13,14] The onset glass transition temperature was observed at ∼136 K using calorimetric measurements, but the underlying nature of the observed increase in heat capacity at this temperature is still controversially discussed.[11]

HDA ice was first discovered by Mishima et al.[6,15] by isothermal compression of hexagonal ice (Ih) at 77 K; the HDA resulting from this procedure is also called unannealed HDA (uHDA). uHDA has ∼20% higher density than LDA. Mishima found an "apparent first-order transition" between LDA and HDA upon compression and decompression.[6] Later, Loerting et al.[16] reported a third form of amorphous ice, made by isobaric heating of HDA above ∼0.8 GPa (up to 160 K). This new amorphous ice has ∼9% higher density than HDA and was therefore called very-high-density amorphous (VHDA) ice.[17] Extensive studies over the last years showed

Received: May 21, 2018
Revised: July 9, 2018
Published: July 23, 2018

DOI: 10.1021/acs.jpcb.8b04823
J. Phys. Chem. B 2018, 122, 7616−7624

that through isothermal decompression of VHDA at 140 K[18,19] or by annealing uHDA at 0.2 GPa to 140 K[20] expanded- or sometimes also called equilibrated-high-density amorphous ice (eHDA) can be produced. eHDA was found to be of greater thermal stability than all other HDA ices.[18,20] A glass−liquid transition was found at ∼116 K for eHDA using different experimental techniques with minor differences in the transition temperature depending on the heating rate.[21] Some alternative interpretations to the proposed transition into HDL include an orientational glass transition.[22] Recently, diffusive dynamics were observed using coherent X-ray diffraction (X-ray photon correlation spectroscopy, XPCS) in the small-angle X-ray scattering (SAXS) geometry when warming HDA above 110 K. On the basis of XPCS and X-ray scattering, an apparent first-order transition into a LDL state was observed.[23]

The structure of amorphous ices has been studied with neutron scattering[24−31] and X-ray diffraction,[25,27,28,31−33] obtaining both the structure factors and the pair-distribution functions (PDFs). Because neutron scattering is dominated by the lighter nuclei, it is most sensitive to the O−H (O−D) and H−H (D−D) interactions. X-rays on the other hand scatter from the electron density and are therefore most sensitive to the O−O and O−H interactions. The scattered intensity is measured as a function of momentum transfer Q, and the structure factor $S(Q)$ can be derived. The structure factor is then Fourier transformed to obtain the PDF. To recover the OO, OH, and HH contributions from neutrons, measurements of three isotopes (H_2O, HDO, and D_2O) are required followed by various simulation methods to disentangle the pair-distributions.[29] From neutron scattering studies, it was found that the amorphous ice structures contain four-coordinated hydrogen-bonded networks with one additional interstitial molecule for HDA and two for VHDA.[17,30]

The goal of the present study is to investigate the O−O PDFs for the amorphous ices LDA, eHDA, and VHDA with wide-angle X-ray scattering (WAXS) at liquid nitrogen temperature (T = 77 K) and ambient pressure. The oxygen−oxygen PDF is determined up to 23 Å for the different amorphous ices. The position of the first coordination shell is determined accurately due to the data going up to high momentum transfer (23 Å^{-1}). The O−O PDFs of the amorphous ices are also compared to those of high-pressure crystalline ices and liquid water in order to investigate potential similarities in the local ordering. At short interatomic distances, similarities are observed between amorphous ices, crystalline ices, and liquid water structures, while in the intermediate range, the peaks in the PDFs of the amorphous ices are significantly broadened, making direct correspondence to the crystalline comparison less pronounced. It is essential to develop models of amorphous ices that can better describe these intermediate-range correlations.

METHODS

Experimental. The measurements were performed at beamline 6 ID-D of the Advanced Photon Source (APS) with an X-ray photon energy of 100 keV and X-ray beam diameter of 0.5 mm. Scattering images were taken using a large 2D amorphous silicon area detector (Perkin-Elmer XRD1621). The Q-calibration was done using a cerium dioxide sample. The angular integration was performed by using FIT2D (V.17.006)[34] software where also polarization and geometrical corrections were taken into account.

As a sample environment we used a liquid N_2-flow cryostat from JANIS, with housing equipped with two Kapton windows (50 μm thickness toward the X-ray and 75 μm toward the detector). The amorphous ice samples were crushed into powder and cold-loaded to the sample holder at liquid nitrogen temperature. In order to keep the sample in place, two Kapton windows (thicknesses of 50 μm) were used, and the effective sample thickness was ∼2 mm with a diameter of 10 mm. The X-ray scattering measurements were performed in vacuum at pressure $P < 1 \times 10^{-2}$ mbar. All measurements shown in this paper were measured at liquid nitrogen temperature. Because the X-ray beam size is smaller than the diameter of the sample, between one and five positions within each sample were measured at liquid nitrogen temperature in order to retrieve better statistics and minimize beam-induced effects (see the Supporting Information for more information).

Sample Preparation. The amorphous ice samples were prepared at Stockholm University by compression, followed by decompression, heating, and annealing at elevated pressures and temperatures 77 < T < 160 K. A mechanical press (Zwick, Z100 TN) was used together with a steel cylinder with cylindrical pistons 10 mm in diameter. uHDA ice was made by pressurizing crystalline ice to 1.6 GPa at liquid nitrogen temperature.[6,20] The uHDA ice was subsequently heated up to 160 K at a constant pressure of 1.1 GPa in order to form VHDA ice. In the next step, VHDA was decompressed to 0.07 GPa at a constant temperature of 140 K,[19] which is slightly above the glass transition temperature (ultraviscous regime, visible in Figure 1 of ref 21), to form eHDA ice.[18] Once the pressure of 0.07 GPa at 140 K was reached, the sample was cooled very rapidly to 77 K by immersion in liquid nitrogen (quench-recovered) to finally obtain eHDA at ambient pressure. If eHDA was instead decompressed further at 140 K to ambient pressure before quenching,[19,35] LDA-II was formed. The samples were stored and shipped at liquid nitrogen temperature. Note that within this paper all eHDA samples will be referred to as HDA and all LDA-II samples will be stated as LDA.

Analysis. The diffraction ring patterns were angularly integrated in reciprocal space to obtain the intensity $I(Q)$ as a function of momentum transfer $Q = 4\pi \sin(\theta)/\lambda$. The background, mainly caused by the Kapton windows, was measured with an empty sample holder and normalized to the sample measured at low Q and then used for subtraction (see Figure 1A). The background was averaged from several independent background measurements at liquid nitrogen temperature. The next step was to normalize the $I(Q)$ to the molecular form factor.[36] The PDFgetX2[37] software was used to retrieve corrections for self-absorption, oblique incidence, and detector efficiency. Multiple scattering was considered but found to have negligible effects on the PDF. The inelastic scattering was corrected for by subtracting the Compton scattering.[38]

The total structure factor was calculated by subtracting the molecular form factor FF(Q)[36] and applying a weighting function WF(Q) from the background-subtracted $I(Q)$, as discussed in detail by Skinner et al.[38]

$$S(Q) - 1 = \frac{I(Q) - \mathrm{FF}(Q)}{\mathrm{WF}(Q)} \quad (1)$$

The weighting function was calculated by using the following expression[38]

DOI: 10.1021/acs.jpcb.8b04823
J. Phys. Chem. B 2018, 122, 7616−7624

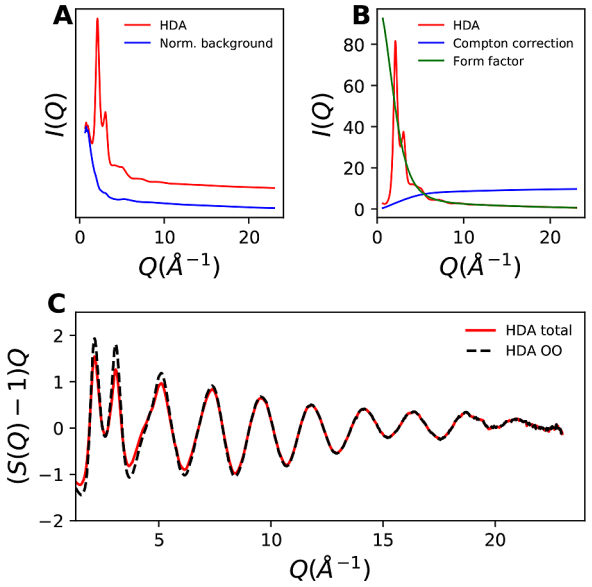

Figure 1. Example of data treatment using an HDA sample. (A) Scaling of the background (blue) to the sample $I(Q)$ (red). (B) $I(Q)$ (red) shown after subtraction of the background (see A) and Compton scattering (blue) plotted together with the molecular form factor (green). (C) Comparison of total structure factor $S(Q)$ (red) and the oxygen−oxygen interaction $S_{OO}(Q)$ (black). To visualize the differences at higher Q, $S(Q)$ is multiplied by Q.

$$\mathrm{WF}(Q) = f_O(Q)^2 + 4f_O(Q)f_H(Q) + 4f_H(Q)^2 \quad (2)$$

where the modified atomic form factors[39] were calculated as

$$f_\alpha(Q) = f_\alpha^O(Q)\left[1 - \frac{a_\alpha}{z_\alpha}\exp(-Q^2/2\beta)\right] \quad (3)$$

with scattering factors $a_H = 0.5$ and $a_O = -1$[40] and $\beta = 2.0$ Å^{-2},[38] where z_α is the number of protons on atom α.

By applying the molecular form factor,[36] all intramolecular interactions were subtracted. The total structure factor $S(Q)$ contains information about the oxygen−oxygen (OO), oxygen−hydrogen (OH), and hydrogen−hydrogen (HH) partial structure factors. In order to calculate the oxygen−oxygen partial structure factor $S_{OO}(Q)$, the following expression was used[38]

$$S_{OO}(Q) = \frac{S(Q) - \omega_{HH} \times 1 - \omega_{OH} \times S_{OH}(Q)}{\omega_{OO}} \quad (4)$$

S_{OH} obtained from oxygen isotope-substituted neutron scattering data for liquid water was used to subtract the OH contribution.[41,42] It has been shown that the detailed shape of the OH contribution is not that important.[38] ω_{xx} are element-specific weighting factors[38] calculated as $\omega_{OO} = f_O^2 \times \mathrm{WF}(Q)^{-1}$, $\omega_{OH} = 4f_Of_H \times WF(Q)^{-1}$, and $\omega_{HH} = 4f_H^2 \times \mathrm{WF}(Q)^{-1}$.

In order to find the PDF $g_{OO}(r)$, the Fourier transform of $S_{OO}(Q)$ was calculated as

$$g_{OO}(r) - 1 = \frac{1}{2\pi^2\rho r}\sum_{Q=0}^{Q_{max}} QS_{OO}(Q)\sin(Qr)\frac{\sin(Q\Delta(r))}{Q\Delta(r)}\,\mathrm{d}Q \quad (5)$$

with ρ being the number density. The function $\Delta(r)$ is an r-dependent averaging width used to reduce high-frequency noise without affecting the shape of the PDF,[43] as defined by Skinner et al.[43]

$$\Delta(r) = a\left(1 - \exp\left(-2.77\left(\frac{r - r_1}{\omega_1}\right)^2\right)\right) + a\left(\frac{1}{2} + \frac{1}{\pi}\arctan\left(\frac{r - \omega_2}{\omega_2/2\pi}\right)\right)\sqrt{r} \quad (6)$$

The constants used were $r_1 = 2.8$ Å, $w_1 = 0.5$ Å, and $w_2 = 12$ Å. Figure 1 shows the data treatment procedure after angular integration described by eqs 1−4 using HDA as an example.

In Figure 1A, the scaling of the background to the sample is shown, which is done in order to subtract the background. In the next step, as seen in Figure 1B, the data are normalized to the molecular form factor of water. The structure factor $S(Q)$ is then retrieved by applying eq 1. In Figure 1C, the total structure factor $S(Q)$ and the oxygen−oxygen, $S_{OO}(Q)$ are compared, whereas $S_{OO}(Q)$ is calculated as shown in eq 4 with the OH contribution subtracted using the measurements on water by Zeidler et al.[41,42] The difference between $S(Q)$ and $S_{OO}(Q)$ are mainly seen at low Q where the $S_{OO}(Q)$ has a higher amplitude.

RESULTS AND DISCUSSION

In this section, the structure factors and PDFs of the different samples are compared and the first peak positions are accurately determined due to the high Q measurements. Figure 2 shows the structure factors $S_{OO}(Q)$ for the three different amorphous ices, namely LDA, HDA, and VHDA. It has been shown before that several substates of the three polyamorphs exist, with subtle differences in the structure but with large differences in thermal stability.[18,35] The samples that we chose for this study are discussed to be the most

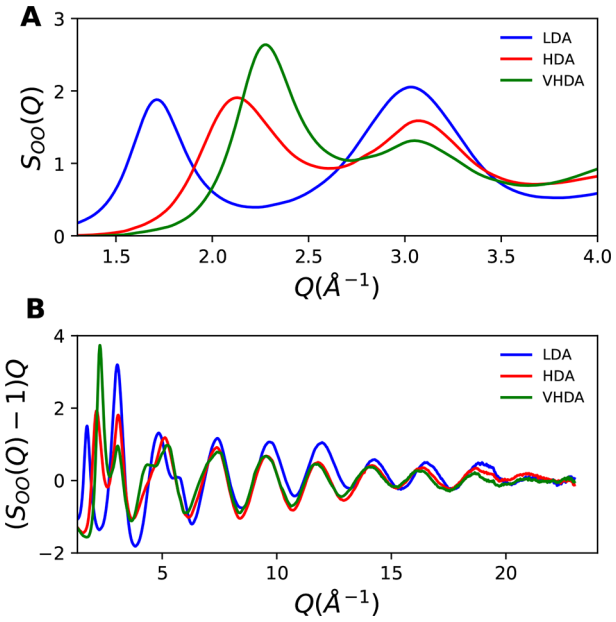

Figure 2. Structure factors at short and intermediate ranges for HDA (=eHDA), LDA (=LDA-II), and VHDA, averaged from individual runs within the same batch (see the SI). (A) First and second maximum in $S(Q)$. (B) Full-range structure factor multiplied by Q. All data are averaged over five sample positions.

DOI: 10.1021/acs.jpcb.8b04823
J. Phys. Chem. B 2018, 122, 7616−7624

equilibrated states,[18,35] i.e., eHDA recovered from 0.07 GPa and 140 K and LDA-II obtained from eHDA at 140 K. VHDA (1.1 GPa/160 K) was obtained following a similar protocol as that for earlier studies.[17,29]

Figure 2A shows the first and second maxima in $S_{OO}(Q)$ for the amorphous ices. In order to find the positions of the first scattering maximum Q_1 in Figure 2A, the data points around the maximum were fitted by a Gaussian function (fixed width of 0.2 Å^{-1}) with resulting maxima Q_1(LDA) = 1.71 Å^{-1}, Q_1(HDA) = 2.14 Å^{-1}, and Q_1(VHDA) = 2.28 Å^{-1}, which shows the difference between the three states and is consistent with values found earlier using X-ray and neutron scattering.[20,29,31,33,44] The position of the second maximum Q_2 instead remains nearly constant for all three amorphous ices at around Q_2 = 3.05 Å^{-1}. The difference between Q_2 and Q_1 is larger for LDA compared to the HDA ices. This is consistent with measurements on supercooled water where it was shown that the increase in splitting of Q_2 and Q_1 is an indication of an increase of tetrahedral structures[45] and therefore is most pronounced in the LDA sample.

In Figure 2B, $(S_{OO}(Q) - 1)Q$ is shown in order to emphasize the oscillations over the full momentum transfer range up to 23 Å^{-1}. The $S(Q) - 1$ converges at intermediate ranges toward zero. It is also seen that all three ice samples follow similar behavior at high Q, even though LDA shows a shift to higher Q, indicating a shorter first-shell distance. Another feature is the maximum at around 5 Å^{-1}, which for LDA shows a shoulder at around 6 Å^{-1} (right side of the maximum), while VHDA has a shoulder at around 4 Å^{-1} (left side of the maximum) and HDA has no pronounced shoulder at all.

Figure 3 shows the oxygen−oxygen PDFs calculated from eqs 5 and 6 with different r-ranges plotted in separate panels to visualize the O−O correlation at higher r. For all ice forms, we

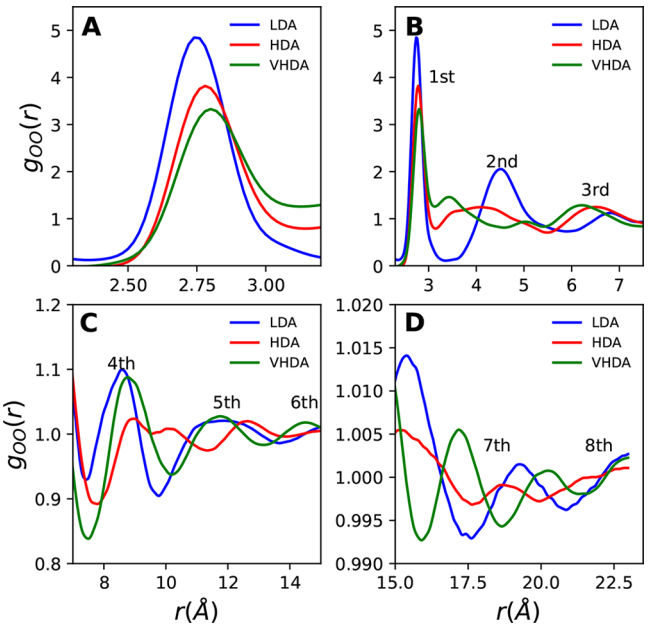

Figure 3. Partial distribution function for oxygen−oxygen interactions for LDA (blue, LDA-II), HDA (red, eHDA), and VHDA (green), averaged from individual runs within the same batch (see the SI). (A) First coordination shell. (B) Short-range correlations. (C) Intermediate-range correlations at 7−15 Å. (D) Intermediate-range correlations at 15−23 Å.

can resolve nearly eight coordination shells due to the wide Q range in the measured $S(Q)$. Figure 3A shows the first coordination shell; plotted data are averaged from individual runs within the same batch (see the SI). To calculate the peak positions, we used a Gaussian fitting (fixed width of 0.2 Å). The peak positions are given in Table 1 together with the first coordination shell position standard deviation. For this calculation, we used all available data sets in order to account for errors caused by sample preparation and sample loading, with a total of 5 runs for LDA, 9 runs for VHDA, and 12 runs on four individual samples for HDA (for more details see the SI).

Table 1. First Coordination Shell Position of $g_{OO}(r)$ and Its Corresponding Standard Deviation (±) and Density[a]

	LDA	HDA	VHDA
r_{OO}	2.750 ± 0.002 Å	2.780 ± 0.005 Å	2.803 ± 0.003 Å
density ρ	0.94[35] g/cm^3	1.13[47] g/cm^3	1.26[16] g/cm^3

[a]To obtain the peak position, all available datasets have been used, in total 5 runs on LDA-II (1 batch), 9 runs on VHDA (1 batch), and 12 runs on eHDA (4 individual batches). Details are given in the SI.

There is a clear shift in the position among LDA, HDA, and VHDA, where the distance to the first nearest oxygen neighbor increases from r = 2.750 Å for LDA to 2.803 Å for VHDA. This might not be intuitive when considering that by applying high pressure the average distance between water molecules should decrease but is consistent with the so-called density−distance paradox[46] where the distance is slightly longer for the high-density phases. The position of the first coordination shell in amorphous ices was previously estimated to be 2.77 (LDA), 2.82 (uHDA), and 2.85 (VHDA) based on Raman spectroscopy measurements.[16] Although the absolute values differ slightly, the general trend of increasing the first peak position is in good agreement with the values presented here. In Figure 3B, the first three coordination shells are shown; the peak at 4.5 Å defines the second coordination shell and is connected to the tetrahedrality of the hydrogen-bond network.[45] LDA (blue) shows the strongest enhancement at that position because it is fully tetrahedrally coordinated. For HDA (red), more interstitial molecules are present between the first and second coordination shells. VHDA (green) shows the smallest degree of tetrahedrality with a substantially increased number of interstitials between the first and second coordination shells. The peak corresponding to the third coordination shell at ∼6.5 Å moves to a shorter distance with increasing density, as seen by the shift to smaller r from LDA to HDA to VHDA. These observations are again consistent with earlier neutron scattering studies.[17,29,30] In Figure 3C, the fourth coordination shell appears to be split in two contributions for HDA. The fourth shells for LDA and VHDA are slightly shifted, while the fifth coordination shell is at the same position even if LDA has a broader feature. LDA and VHDA seem to be in phase in the intermediate range. HDA on the other hand has its fourth coordination shell clearly shifted to longer distances but shows instead a very broad feature due to a double peak, which appears similarly in experimental liquid water at a temperature of 365.9 K (as discussed later). The fifth coordination shell for HDA is shifted to longer distances than that for LDA and VHDA. In Figure 3D, the $g_{OO}(r)$ has been plotted up to 23 Å, and in this range, clear structures can be seen where VHDA and LDA have opposite periodicity.

DOI: 10.1021/acs.jpcb.8b04823
J. Phys. Chem. B 2018, 122, 7616−7624

In order to determine the number of atoms as a function of distance r, the oxygen−oxygen running coordination number $n_{OO}(r)$ was calculated by integrating the PDF[29,35,43]

$$n_{OO}(r) = 4\pi\rho \int_0^r r^2 g(r)\, dr \tag{7}$$

where ρ is the number density for the specific sample. In Figure 4A, the $n_{OO}(r)$ for LDA shows a plateau around four

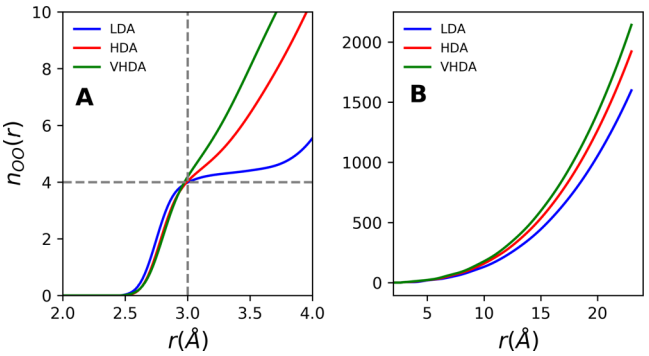

Figure 4. Running O−O coordination number of LDA (blue), HDA (red), and VHDA (green). (A) Short-range. (B) Full range.

molecules that is due to the tetrahedral structure and lack of interstitials, as also seen previously by neutron scattering experiments on amorphous ices.[29] For HDA and VHDA, there is no plateau visible; instead, the running coordination number increases further due to the presence of interstitial molecules. In the same range as the plateau of LDA, VHDA has one more molecule than HDA, which can be related to the addition of a second interstitial molecule.[17] The coordination number 5 for HDA and 6 for VHDA is estimated in the range between r = 2 and 3.25 Å, which is fully consistent with earlier neutron scattering studies showing the same value in the range between 2.5 and 3.3 Å.[17,29,30] By doing the integration this way, one defines the size of the so-called first coordination shell to have a fixed range when comparing the different amorphous ices; this choice is somewhat arbitrary. However, it is worth noting that X-ray and neutron scattering measurements obtain the same coordination numbers when using the same procedure. In Figure 4B, the full range out to intermediate distances is shown with the expected density dependence.

Comparison with Crystalline Ices and Liquid Water. In this section, we discuss the relation of the amorphous ice structures to different crystalline ice phases as well as to liquid water. LDA is a low-pressure form and is thus compared with hexagonal ice because it is the stable form of ice at ambient pressure. Upon isobaric heating of HDA at a pressure of 0.51 GPa, it transforms into ice IX,[48−50] which is a metastable high-pressure ice with similar density (1.16 g/cm^3) as HDA (1.13 g/cm^3). Recently, HDA has also been discussed to be a "derailed" state on the ice I to ice IV pathway.[51] Therefore, we compare HDA to both ice IX and ice IV. The metastable high-pressure ice XII can be formed by isobaric heating of HDA at a pressure of 0.81 GPa up to 183 K and has a density of 1.30 g/cm^3 and is therefore most similar to VHDA.[52−55] The PDFs of the crystalline ices shown in Figure 5 were calculated from their lattice parameters,[56−58] where the initial unit cells were expanded to reach intermediate distances for calculating the PDF. In addition, disorder was introduced by random displacements assuming a Gaussian distribution with width

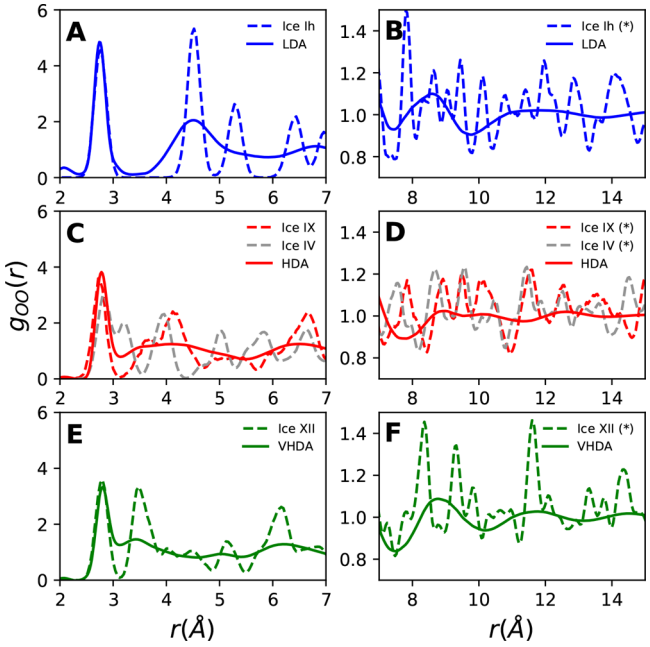

Figure 5. Oxygen−oxygen distribution function of amorphous ice (solid line) compared with crystalline ice (dashed) calculated from structure models. (A,B) LDA and hexagonal ice. (C,D) HDA, ice IX, and ice IV. (E,F) VHDA and ice XII. In panels (B), (D), and (F), the crystalline data are scaled by a factor of 1/3 and shifted upward by 0.7 for better comparison.

0.08 Å (based on the reported mean-square displacement for ice Ih[59]), resulting in broadening, similar to previous approaches.[28]

In Figure 5A, the short-range PDF comparison shows that both LDA and hexagonal ice exhibit first and second coordination shells in the same range, but the third and fourth maxima caused by hexagonal geometries are not as clear in LDA due to potential contributions of other local structures than six-member rings. At longer distances shown in Figure 5B, the LDA maximum at ∼9 Å is shifted from the pronounced maximum observed for hexagonal ice at ∼7.5 Å. In Figure 5C, HDA is compared to ice IX and ice IV. The first coordination shell in HDA is slightly shifted to larger distances and distinctly broadened compared to ice IX, reflecting a large degree of disorder in the amorphous state. Both HDA and ice IX exhibit interstitial water molecules located between the first and second coordination shells. Ice IV instead shows an additional peak at 3.2 Å where HDA and ice IX have a minimum in $g(r)$ between the first and second shells. The third coordination shell of HDA is at the same position as the fourth coordination shell of ice IX. In Figure 5D, ice IX shows a maximum of ∼7.5 Å where HDA has a minimum. Ice IV and IX show three maxima in the range of 9−11 Å where the fourth coordination shell of HDA shows a double-peak feature. At longer distances, the two crystalline states become more similar, while the PDF of HDA broadens even more. In Figure 5E, it is evident that the interstitials for ice XII are at an even shorter distance, which is most similar to VHDA. There is a maximum at 6 Å, which is also seen in VHDA. In Figure 5F, the two peaks for ice XII at 8−10 Å are underlying a broad maximum in VHDA. Therefore, we observe that all intermediate ranges plotted in Figure 5B,D,F show pronounced differences between the crystalline and amorphous ices due to the large degree of disorder in the amorphous states. However, the broad features

DOI: 10.1021/acs.jpcb.8b04823
J. Phys. Chem. B 2018, 122, 7616−7624

in the amorphous states could be interpreted as broadening of the crystalline peaks. Thus, we conclude that local structural similarities between ice phases and amorphous states are found up to a length scale of about 8 Å, while beyond that the peaks in the amorphous ice PDFs are significantly broadened but exhibit intensity at similar distances as the crystalline comparisons.

In the case of liquid water, it has been proposed that warm water is more of high-density structure in terms of higher coordination shells, while upon cooling low-density structures appear as fluctuations[2] that are further enhanced upon supercooling.[45,60] The liquid counterparts to the amorphous HDA and LDA are discussed to be HDL and LDL, respectively.[2] The intermediate-range correlations of HDL- and LDL-like water derived at different temperatures was studied previously based on X-ray scattering and molecular dynamics simulations[61] and are compared to the amorphous ices in Figure 6.

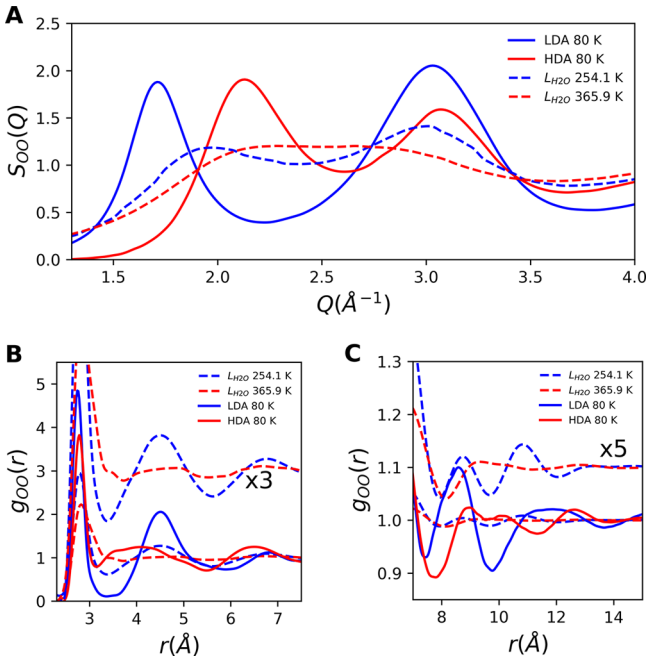

Figure 6. Liquid water comparison with LDA and HDA. (A) Structure factor. (B) Short-range PDF. (C) Intermediate-range PDF. At short range, the liquid water data was multiplied by 3 and at intermediate range the liquid water was multiplied by 5 in order to magnify the structures for better visibility.

In Figure 6A, the $S_{OO}(Q)$ is shown for LDA (blue line) and liquid water at 254.1 K (blue dashed). Here we emphasize the splitting between the first and second diffraction peaks Q_1 and Q_2, which appears less pronounced for water at higher temperatures (365.9 K, red dashed) and also for HDA (red line). Upon supercooling water, the first diffraction peak shifts toward the LDA position, as seen previously in the deeply supercooled region.[45] In Figure 6B, the radial distribution functions $g_{OO}(r)$ are shown for all amorphous and liquid states, where the curves for liquid water are magnified by a factor of 3 for better comparison. It can be seen that, up to distances of around 10 Å, the O−O PDF of LDA is similar to that of liquid water at supercooled temperatures. HDA and liquid water at warm temperatures also show similarity; however, it is less pronounced in the first and second shells (<6 Å), but they agree astonishingly well in the intermediate range of $7 < r < 15$ Å (Figure 6C). In Figure 6C, the data for liquid water are multiplied by a factor of 5, which makes it clearer that the broad feature at around 9−10 Å seen for HDA is similar to that for liquid water at a temperature of 365.9 K. Comparing instead LDA and liquid water at 254.1 K at intermediate ranges, the maximum at around 8.5 Å for liquid water is shifted to slightly longer distances, while for peaks at longer distance, the differences become larger.

VHDA is produced at a very high pressure of 1.1 GPa and resembles the amorphous ices of highest density; therefore, it is compared in Figure 7 with experimental data of high-pressure

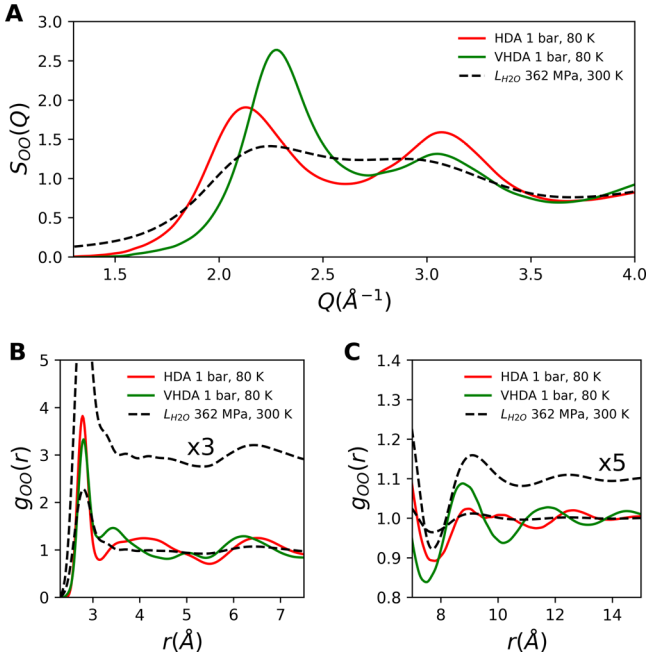

Figure 7. Comparison of experimental high-pressure liquid water from Skinner et al.[62] with HDA data. (A) Structure factor. (B) Short-range PDF. (C) Intermediate-range PDF.

liquid water from Skinner et al.[62] The high-pressure liquid water data are obtained at ambient temperature where the water sample was 2.5 mm thick and confined between two single-crystal diamond windows.[62]

In Figure 7A, the structure factor $S_{OO}(Q)$ is shown for the first two diffraction peaks for high-pressure water at 362 MPa (black dashed), HDA (red), and VHDA (green). The Q_1 position for high-pressure water lies between that of HDA and VHDA, whereas Q_2 is shifted to a smaller value. The difference between Q_1 and Q_2 in high-pressure water is thus smaller, indicating a less tetrahedral structure. In Figure 7B, we compare the pair-correlation function $g(r)$ of high-pressure water with that of HDA and VHDA, where the water data are additionally plotted magnified by a factor of 3 for comparison. The first coordination shell is at about the same position as that for HDA and VHDA. Skinner et al.[62] compared ambient water with high-pressure water, showing large structural differences in the region above 3 Å associated with the collapse of the well-defined second shell and shifting of higher shells to shorter distances with pressure. This is also visible in Figure 7B; the second coordination shell is not distinct for the high-pressure water, which is consistent with HDA and, in particular, VHDA, having interstitial positions occupied

DOI: 10.1021/acs.jpcb.8b04823
J. Phys. Chem. B 2018, 122, 7616−7624

between the first and second coordination shells. In Figure 7C, the high-pressure water data at intermediate ranges ($5.5 < r < 15$ Å) is similar to that of VHDA but shifted to longer distances. When comparing to HDA, the maximum at around 6 Å is at the same position, but the broad feature seen for HDA at around 9−10 Å was not seen for the high-pressure data. The maximum in HDA at around 12.5 Å overlaps with the high-pressure data. In general, we conclude that the PDF of liquid water at high pressures shows similarities with both VHDA and HDA ices but is quite distinct from LDA.

CONCLUSIONS

In this study, intermediate-range correlations are determined for the amorphous ices LDA, HDA, and VHDA up to distances of r = 23 Å. The different amorphous ice forms are also compared to crystalline ices and liquid water at different pressures and temperatures. The O−O PDF of LDA ice exhibits the strongest enhancement at r = 4.5 Å because it is tetrahedrally coordinated, whereas HDA and VHDA exhibit increased presence of interstitial molecules between the first and second coordination shells. On the other hand, at intermediate ranges (7−12 Å), the PDFs of LDA and VHDA are similar, while that of HDA is very different with a distinct feature at around ∼9−10 Å, which is also seen for liquid water at 365.9 K. In the range of 15−23 Å, the PDFs of VHDA and LDA appear out of phase, contrary to HDA and LDA, which exhibit similar ordering. Comparison of the amorphous forms LDA, HDA, and VHDA with crystalline ices Ih, IV, IX, and XII indicates that, even though the crystalline forms are similar to the corresponding amorphous ices at shorter distances (first and second coordination shell), the intermediate regime is significantly broadened due to the disorder in the amorphous states. On the other hand, comparison with liquid water in the supercooled regime or at elevated pressures exhibits much better qualitative agreement with the respective amorphous ice forms. In supercooled water at 254.1 K, fluctuations into low-density local structures are significant,[45,60] while hot water is more of a high-density structure. From the comparison, we can conclude that the corresponding local structures are similar to the respective amorphous ices up to around 10 Å. High-pressure liquid water on the other hand is structurally most similar to HDA and VHDA.

As already discussed in the Introduction of this paper, the nature of the amorphous ices has been discussed controversially for decades.[3−5] On one hand, the amorphous ices are proposed to be the glassy counterparts of two distinct liquid states, i.e., LDL and HDL.[3,6,8] On the other hand, amorphous ices, in particular, those coming from HDA as the starting material, are discussed to be a collapsed crystal[63,64] and of nanocrystalline nature[65] or rather a derailed crystalline state.[51] Although the increase in heat capacity observed in calorimetric studies has been interpreted as a glass-to-liquid transition,[21] others discuss this experimental observation as reorientational dynamics in the solid state.[22] However, in the present study, we cannot draw direct conclusions about the dynamics in the amorphous ices because we exclusively look at the structural data using WAXS. Still it is worth comparing the structural data of the amorphous ices with those of different crystalline phases as well as liquid water at different temperatures.[30]

In an earlier study, Guthrie et al.[28] compared different HDA ices with the high-pressure crystalline ices XII and VI. The authors concluded that VHDA is not a nanocrystalline ice form, but still, there are similarities to ice XII and VI in their short-range structure. The results of the present study are in agreement with these earlier conclusions in that our comparison with crystalline ices finds most similarities between LDA and hexagonal ice, HDA and ice IX, and VHDA and ice XII below 8 Å. Above 8 Å, the peaks in the PDFs of the amorphous ices become significantly broadened, and hence, the potential structural similarity between amorphous and crystalline ices becomes less evident. As expected, the amorphous ices lack long-range order in contrast to crystalline ices. In order to understand which local structures exist in amorphous ice, improved simulation models will be valuable.

ASSOCIATED CONTENT

Supporting Information

The Supporting Information is available free of charge on the ACS Publications website at DOI: 10.1021/acs.jpcb.8b04823.

Table of all samples used, discussion and figures about the uncertainty of the measurements, i.e., scattering within different samples of the same species, a figure comparing our X-ray data with neutron scattering data available in literature, and a figure comparing different LDA states (PDF)

ASCII files for $S(Q)$ and $g(r)$ are available (ZIP)

AUTHOR INFORMATION

Corresponding Author

*E-mail: katrin.amannwinkel@fysik.su.se. Phone: +46855378700.

ORCID

Anders Nilsson: 0000-0003-1968-8696

Katrin Amann-Winkel: 0000-0002-7319-7807

Notes

The authors declare no competing financial interest.

ACKNOWLEDGMENTS

We acknowledge financial support from the European Research Council Advanced Grant WATER under Project (667205) and the Swedish Research Council. This research used resources of the Advanced Photon Source, a U.S. Department of Energy (DOE) Office of Science by Argonne National Laboratory under Contract DE-AC02-06CH11357.

REFERENCES

(1) Debenedetti, P. G. Supercooled and glassy water. *J. Phys.: Condens. Matter* **2003**, *15*, R1669.

(2) Nilsson, A.; Pettersson, L. G. The structural origin of anomalous properties of liquid water. *Nat. Commun.* **2015**, *6*, 8998.

(3) Gallo, P.; Amann-Winkel, K.; Angell, C. A.; Anisimov, M. A.; Caupin, F.; Chakravarty, C.; Lascaris, E.; Loerting, T.; Panagiotopoulos, A. Z.; Russo, J.; et al. Water: A tale of two liquids. *Chem. Rev.* **2016**, *116*, 7463−7500.

(4) Limmer, D. T.; Chandler, D. The putative liquid-liquid transition is a liquid-solid transition in atomistic models of water. *J. Chem. Phys.* **2011**, *135*, 134503.

(5) Caupin, F. Escaping the no man's land: Recent experiments on metastable liquid water. *J. Non-Cryst. Solids* **2015**, *407*, 441−448.

(6) Mishima, O.; Calvert, L.; Whalley, E. An apparently first-order transition between two amorphous phases of ice induced by pressure. *Nature* **1985**, *314*, 76−78.

(7) Mishima, O.; Stanley, H. E. The relationship between liquid, supercooled and glassy water. *Nature* **1998**, *396*, 329.

DOI: 10.1021/acs.jpcb.8b04823
J. Phys. Chem. B 2018, 122, 7616−7624

(8) Poole, P. H.; Sciortino, F.; Essmann, U.; Stanley, H. E. Phase behaviour of metastable water. *Nature* **1992**, *360*, 324−328.
(9) Palmer, J. C.; Martelli, F.; Liu, Y.; Car, R.; Panagiotopoulos, A. Z.; Debenedetti, P. G. Metastable liquid−liquid transition in a molecular model of water. *Nature* **2014**, *510*, 385.
(10) Debenedetti, P. G. Condensed matter: One substance, two liquids? *Nature* **1998**, *392*, 127.
(11) Amann-Winkel, K.; Böhmer, R.; Fujara, F.; Gainaru, C.; Geil, B.; Loerting, T. Colloquium: Water's controversial glass transitions. *Rev. Mod. Phys.* **2016**, *88*, 011002.
(12) McMillan, J.; Los, S. Vitreous ice: Irreversible transformations during warm-up. *Nature* **1965**, *206*, 806.
(13) Brüggeller, P.; Mayer, E. Complete vitrification in pure liquid water and dilute aqueous solutions. *Nature* **1980**, *288*, 569−571.
(14) Hallbrucker, A.; Mayer, E.; Johari, G. Glass-liquid transition and the enthalpy of devitrification of annealed vapor-deposited amorphous solid water: a comparison with hyperquenched glassy water. *J. Phys. Chem.* **1989**, *93*, 4986−4990.
(15) Mishima, O.; Calvert, L.; Whalley, E. 'Melting ice'I at 77 K and 10 kbar: a new method of making amorphous solids. *Nature* **1984**, *310*, 393.
(16) Loerting, T.; Salzmann, C.; Kohl, I.; Mayer, E.; Hallbrucker, A. A second distinct structural "state" of high-density amorphous ice at 77 K and 1 bar. *Phys. Chem. Chem. Phys.* **2001**, *3*, 5355−5357.
(17) Finney, J.; Bowron, D.; Soper, A.; Loerting, T.; Mayer, E.; Hallbrucker, A. Structure of a new dense amorphous ice. *Phys. Rev. Lett.* **2002**, *89*, 205503.
(18) Winkel, K.; Mayer, E.; Loerting, T. Equilibrated high-density amorphous ice and its first-order transition to the low-density form. *J. Phys. Chem. B* **2011**, *115*, 14141−14148.
(19) Winkel, K.; Elsaesser, M. S.; Mayer, E.; Loerting, T. Water polyamorphism: reversibility and (dis) continuity. *J. Chem. Phys.* **2008**, *128*, 044510.
(20) Nelmes, R. J.; Loveday, J. S.; Strässle, T.; Bull, C. L.; Guthrie, M.; Hamel, G.; Klotz, S. Annealed high-density amorphous ice under pressure. *Nat. Phys.* **2006**, *2*, 414−418.
(21) Amann-Winkel, K.; Gainaru, C.; Handle, P. H.; Seidl, M.; Nelson, H.; Böhmer, R.; Loerting, T. Water's second glass transition. *Proc. Natl. Acad. Sci. U. S. A.* **2013**, *110*, 17720−17725.
(22) Shephard, J.; Salzmann, C. Molecular reorientation dynamics govern the glass transitions of the amorphous ices. *J. Phys. Chem. Lett.* **2016**, *7*, 2281−2285.
(23) Perakis, F.; Amann-Winkel, K.; Lehmkühler, F.; Sprung, M.; Mariedahl, D.; Sellberg, J. A.; Pathak, H.; Späh, A.; Cavalca, F.; Schlesinger, D.; et al. Diffusive dynamics during the high-to-low density transition in amorphous ice. *Proc. Natl. Acad. Sci. U. S. A.* **2017**, *114*, 8193−8198.
(24) Koza, M.; Schober, H.; Fischer, H.; Hansen, T.; Fujara, F. Kinetics of the high-to low-density amorphous water transition. *J. Phys.: Condens. Matter* **2003**, *15*, 321.
(25) Tulk, C.; Benmore, C.; Urquidi, J.; Klug, D.; Neuefeind, J.; Tomberli, B.; Egelstaff, P. Structural studies of several distinct metastable forms of amorphous ice. *Science* **2002**, *297*, 1320−1323.
(26) Koza, M. M.; Geil, B.; Winkel, K.; Koehler, C.; Czeschka, F.; Scheuermann, M.; Schober, H.; Hansen, T. Nature of amorphous polymorphism of water. *Phys. Rev. Lett.* **2005**, *94*, 125506.
(27) Guthrie, M.; Urquidi, J.; Tulk, C. A.; Benmore, C. J.; Klug, D. D.; Neuefeind, J. Direct structural measurements of relaxation processes during transformations in amorphous ice. *Phys. Rev. B: Condens. Matter Mater. Phys.* **2003**, *68*, 184110.
(28) Guthrie, M.; Tulk, C. A.; Benmore, C. J.; Klug, D. D. A structural study of very high-density amorphous ice. *Chem. Phys. Lett.* **2004**, *397*, 335−339.
(29) Bowron, D.; Finney, J.; Hallbrucker, A.; Kohl, I.; Loerting, T.; Mayer, E.; Soper, A. The local and intermediate range structures of the five amorphous ices at 80 K and ambient pressure: A Faber-Ziman and Bhatia-Thornton analysis. *J. Chem. Phys.* **2006**, *125*, 194502.
(30) Finney, J.; Hallbrucker, A.; Kohl, I.; Soper, A.; Bowron, D. Structures of high and low density amorphous ice by neutron diffraction. *Phys. Rev. Lett.* **2002**, *88*, 225503.
(31) Amann-Winkel, K.; Bellissent-Funel, M.-C.; Bove, L. E.; Loerting, T.; Nilsson, A.; Paciaroni, A.; Schlesinger, D.; Skinner, L. X-ray and neutron scattering of water. *Chem. Rev.* **2016**, *116*, 7570−7589.
(32) Tse, J. S.; Klug, D. D.; Guthrie, M.; Tulk, C. A.; Benmore, C. J.; Urquidi, J. Investigation of the intermediate- and high-density forms of amorphous ice by molecular dynamics calculations and diffraction experiments. *Phys. Rev. B: Condens. Matter Mater. Phys.* **2005**, *71*, 214107.
(33) Bizid, A.; Bosio, L.; Defrain, A.; Oumezzine, M. Structure of high-density amorphous water. I. X-ray diffraction study. *J. Chem. Phys.* **1987**, *87*, 2225−2230.
(34) Hammersley, A.; Svensson, S.; Hanfland, M.; Fitch, A.; Hausermann, D. Two-dimensional detector software: from real detector to idealised image or two-theta scan. *High Pressure Res.* **1996**, *14*, 235−248.
(35) Winkel, K.; Bowron, D.; Loerting, T.; Mayer, E.; Finney, J. Relaxation effects in low density amorphous ice: Two distinct structural states observed by neutron diffraction. *J. Chem. Phys.* **2009**, *130*, 204502.
(36) Wang, J.; Tripathi, A. N.; Smith, V. H., Jr Chemical binding and electron correlation effects in x-ray and high energy electron scattering. *J. Chem. Phys.* **1994**, *101*, 4842−4854.
(37) Qiu, X.; Thompson, J. W.; Billinge, S. J. PDFgetX2: a GUI-driven program to obtain the pair distribution function from X-ray powder diffraction data. *J. Appl. Crystallogr.* **2004**, *37*, 678−678.
(38) Skinner, L. B.; Huang, C.; Schlesinger, D.; Pettersson, L. G.; Nilsson, A.; Benmore, C. J. Benchmark oxygen-oxygen pair-distribution function of ambient water from x-ray diffraction measurements with a wide Q-range. *J. Chem. Phys.* **2013**, *138*, 074506.
(39) Sorenson, J. M.; Hura, G.; Glaeser, R. M.; Head-Gordon, T. What can x-ray scattering tell us about the radial distribution functions of water? *J. Chem. Phys.* **2000**, *113*, 9149−9161.
(40) Su, Z.; Coppens, P. Relativistic x-ray elastic scattering factors for neutral atoms Z= 1−54 from multiconfiguration Dirac−Fock wavefunctions in the 0−12Å− 1 $\sin\theta/\lambda$ range, and six-Gaussian analytical expressions in the 0−6Å− 1 range. *Acta Crystallogr., Sect. A: Found. Crystallogr.* **1997**, *53*, 749−762.
(41) Zeidler, A.; Salmon, P. S.; Fischer, H. E.; Neuefeind, J. C.; Simonson, J. M.; Lemmel, H.; Rauch, H.; Markland, T. E. Oxygen as a site specific probe of the structure of water and oxide materials. *Phys. Rev. Lett.* **2011**, *107*, 145501.
(42) Zeidler, A.; Salmon, P. S.; Fischer, H. E.; Neuefeind, J. C.; Simonson, J. M.; Markland, T. E. Isotope effects in water as investigated by neutron diffraction and path integral molecular dynamics. *J. Phys.: Condens. Matter* **2012**, *24*, 284126.
(43) Skinner, L. B.; Benmore, C.; Neuefeind, J.; Parise, J. The structure of water around the compressibility minimum. *J. Chem. Phys.* **2014**, *141*, 214507.
(44) Bellissent-Funel, M.; Bosio, L.; Hallbrucker, A.; Mayer, E.; Sridi-Dorbez, R. X-ray and neutron scattering studies of the structure of hyperquenched glassy water. *J. Chem. Phys.* **1992**, *97*, 1282−1286.
(45) Sellberg, J. A.; Huang, C.; McQueen, T. A.; Loh, N.; Laksmono, H.; Schlesinger, D.; Sierra, R.; Nordlund, D.; Hampton, C.; Starodub, D.; et al. Ultrafast X-ray probing of water structure below the homogeneous ice nucleation temperature. *Nature* **2014**, *510*, 381−384.
(46) Okhulkov, A.; Demianets, Y. N.; Gorbaty, Y. E. X-ray scattering in liquid water at pressures of up to 7.7 kbar: Test of a fluctuation model. *J. Chem. Phys.* **1994**, *100*, 1578−1588.
(47) Loerting, T.; Winkel, K.; Seidl, M.; Bauer, M.; Mitterdorfer, C.; Handle, P. H.; Salzmann, C. G.; Mayer, E.; Finney, J. L.; Bowron, D. T. How many amorphous ices are there? *Phys. Chem. Chem. Phys.* **2011**, *13*, 8783−8794.
(48) Seidl, M.; Fayter, A.; Stern, J. N.; Zifferer, G.; Loerting, T. Shrinking water's no man's land by lifting its low-temperature

DOI: 10.1021/acs.jpcb.8b04823
J. Phys. Chem. B 2018, 122, 7616−7624

boundary. *Phys. Rev. B: Condens. Matter Mater. Phys.* **2015**, *91*, 144201.
(49) Salzmann, C. G.; Loerting, T.; Klotz, S.; Mirwald, P. W.; Hallbrucker, A.; Mayer, E. Isobaric annealing of high-density amorphous ice between 0.3 and 1.9 GPa: in situ density values and structural changes. *Phys. Chem. Chem. Phys.* **2006**, *8*, 386−397.
(50) Tonauer, C. M.; Seidl-Nigsch, M.; Loerting, T. High-density amorphous ice: nucleation of nanosized low-density amorphous ice. *J. Phys.: Condens. Matter* **2018**, *30*, 034002.
(51) Shephard, J. J.; Ling, S.; Sosso, G. C.; Michaelides, A.; Slater, B.; Salzmann, C. G. Is high-density amorphous ice simply a "derailed" state along the ice I to ice IV pathway? *J. Phys. Chem. Lett.* **2017**, *8*, 1645−1650.
(52) Salzmann, C. G.; Kohl, I.; Loerting, T.; Mayer, E.; Hallbrucker, A. Pure ices IV and XII from high-density amorphous ice. *Can. J. Phys.* **2003**, *81*, 25−32.
(53) Koza, M.; Schober, H.; Tölle, A.; Fujara, F.; Hansen, T. Formation of ice XII at different conditions. *Nature* **1999**, *397*, 660.
(54) Koza, M. M.; Schober, H.; Hansen, T.; Tölle, A.; Fujara, F. Ice XII in its second regime of metastability. *Phys. Rev. Lett.* **2000**, *84*, 4112.
(55) Stern, J.; Loerting, T. Crystallisation of the amorphous ices in the intermediate pressure regime. *Sci. Rep.* **2017**, *7*, 3995.
(56) Röttger, K.; Endriss, A.; Ihringer, J.; Doyle, S.; Kuhs, W. Lattice constants and thermal expansion of H2O and D2O ice Ih between 10 and 265 K. *Acta Crystallogr., Sect. B: Struct. Sci.* **1994**, *50*, 644−648.
(57) Londono, J.; Kuhs, W.; Finney, J. Neutron diffraction studies of ices III and IX on under-pressure and recovered samples. *J. Chem. Phys.* **1993**, *98*, 4878−4888.
(58) Lobban, C.; Finney, J.; Kuhs, W. The structure of a new phase of ice. *Nature* **1998**, *391*, 268−270.
(59) Koza, M. M.; Geil, B.; Schober, H.; Natali, F. Absence of molecular mobility on nano-second time scales in amorphous ice phases. *Phys. Chem. Chem. Phys.* **2005**, *7*, 1423−1431.
(60) Kim, K. H.; Späh, A.; Pathak, H.; Perakis, F.; Mariedahl, D.; Amann-Winkel, K.; Sellberg, J. A.; Lee, J. H.; Kim, S.; Park, J.; et al. Maxima in the thermodynamic response and correlation functions of deeply supercooled water. *Science* **2017**, *358*, 1589−1593.
(61) Schlesinger, D.; Wikfeldt, K. T.; Skinner, L. B.; Benmore, C. J.; Nilsson, A.; Pettersson, L. G. The temperature dependence of intermediate range oxygen-oxygen correlations in liquid water. *J. Chem. Phys.* **2016**, *145*, 084503.
(62) Skinner, L. B.; Galib, M.; Fulton, J. L.; Mundy, C. J.; Parise, J. B.; Pham, V.-T.; Schenter, G. K.; Benmore, C. J. The structure of liquid water up to 360 MPa from x-ray diffraction measurements using a high Q-range and from molecular simulation. *J. Chem. Phys.* **2016**, *144*, 134504.
(63) Tse, J. S. Mechanical instability in ice I h. A mechanism for pressure-induced amorphization. *J. Chem. Phys.* **1992**, *96*, 5482−5487.
(64) Tse, J.; Klug, D.; Tulk, C.; Swainson, I.; Svensson, E.; Loong, C.-K.; Shpakov, V.; Belosludov, V.; Belosludov, R.; Kawazoe, Y. The mechanisms for pressure-induced amorphization of ice I h. *Nature* **1999**, *400*, 647.
(65) Machon, D.; Meersman, F.; Wilding, M.; Wilson, M.; McMillan, P. Pressure-induced amorphization and polyamorphism: Inorganic and biochemical systems. *Prog. Mater. Sci.* **2014**, *61*, 216−282.

DOI: 10.1021/acs.jpcb.8b04823
J. Phys. Chem. B 2018, 122, 7616−7624